ACS APPLIED MATERIALS & INTERFACES

www.acsami.org

Research Article

Bottom-Up Fabrication of Large-Scale Gold Nanorod Arrays by Surface Diffusion-Mediated DNA Origami Assembly

Shuo Yang, Wenyan Liu, Yuwei Zhang, and Risheng Wang*

Cite This: *ACS Appl. Mater. Interfaces* 2021, 13, 50516–50523

Read Online

ACCESS | Metrics & More | Article Recommendations | Supporting Information

ABSTRACT: Self-assembly of anisotropic metal nanoparticles serves as an effective bottom-up route for the nanofabrication of novel artifacts. However, there still are many challenges to rationally manipulate anisotropic particles due to the size and geometric restrictions. To avoid the aggregation and mishybridization from DNA sticky-end-guided assembly in buffer solution, in this work, we utilized a cation-controlled surface diffusion strategy to the spatial arrangement of gold nanorods (AuNRs) into 1D and 2D arrays by using DNA origami tiles as binding frames on the solid−liquid interface through $\pi-\pi$ stacking interactions. To facilitate the further manipulation of those patterns, a novel pattern transfer method was introduced to transfer the arrays of AuNRs from a liquid to a dry ambient environment with high yield and minor structural damage. The results demonstrated a successful strategy of DNA origami-assisted, large-scale assembly of AuNRs for constructing complex superstructures with potential applications in the nanofabrication of plasmonic and electronic devices.

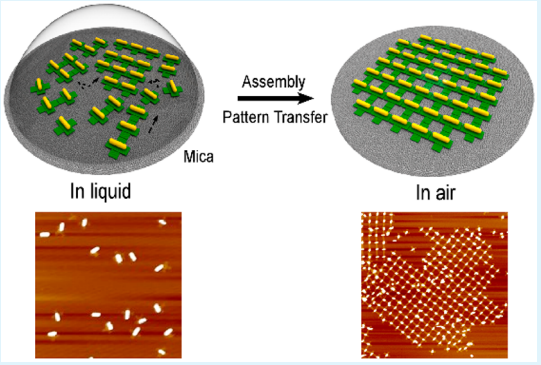

KEYWORDS: *DNA origami, self-assembly, gold nanorods, anisotropic nanoparticles, 2D arrays*

INTRODUCTION

The self-assembly of nanoparticles is a rapidly developing field of research geared toward the fabrication of unique mesostructured materials with intrinsic properties.[1] Anisotropic nanoparticles have been of particular interest recently because of their tunable physical and optical properties based on the unique anisotropic geometries. For example, the gold nanorods (AuNRs) can be synthesized with varied dimensions, which exhibit finely tunable plasmonic features from visible to near-IR regions.[2] Despite tremendous advances, the manipulation of anisotropic nanoparticles into rationally designed ensembles remains the most significant challenge because it requires not only control over the positions of the nanoparticles but over their orientations as well. AuNRs tend to form tip-to-tip, side-by-side ensembles, either in colloidal solution or patterned substrates.[3,4] It is critical that such pattern limitations be overcome to create diverse and rational controlled AuNR arrays with nanometer precision.

DNA-directed self-assembly[5,6] of nanomaterials has shown great potential as a powerful tool for the fabrication of various functional nanostructures because of the advantages of high yield, superior addressability, and precise positioning, which have been employed for many applications such as biosensing,[7,8] nanomedicine,[9−11] and nanoelectronics.[12−14] In particular, extensive research has focused on utilizing DNA origami[15] as building blocks for the assembly of plasmonic metallic nanostructures from AuNRs.[16,17] For instance, AuNRs that are precisely arranged into one-dimensional (1D) plasmonic polymers are capable of transporting plasmonic angular momentum and magnetic surface plasmonic polaritons.[18] Besides, the dynamic tuning of AuNRs helixes by V-shaped DNA origami can produce plasmonic chiral superstructures with switchable chirality.[19] Other examples include dynamic walker,[20] reconfigurable AuNR tripods,[21] as well as heterogeneous plasmonic metamolecules.[22] For most nanostructures mentioned above, mishybridization between DNA origami units guided by sticky-ended cohesion is one of the major technical obstacles during the fabrication process, which leads to disordered aggregates, lowered productive yield, and limited size of AuNR assemblies or clusters. Besides that, these nanostructures are generally formed in a test tube, then deposited onto substrates for characterization and further processing, which inevitably leads to structural distortion and damage during deposition.[22,23] To address these issues, assembling nanostructures directly on substrates may provide a route for making more reproducible patterns.[24−27] In such a process, DNA origami units are dynamically reorganized on

Received: July 12, 2021
Accepted: September 27, 2021
Published: October 12, 2021

https://doi.org/10.1021/acsami.1c13173
ACS Appl. Mater. Interfaces 2021, 13, 50516−50523

Scheme 1. Schematic Illustration of the Strategy for Constructing the Origami Framed AuNRs and Assembling AuNRs into 2D Nanostructures

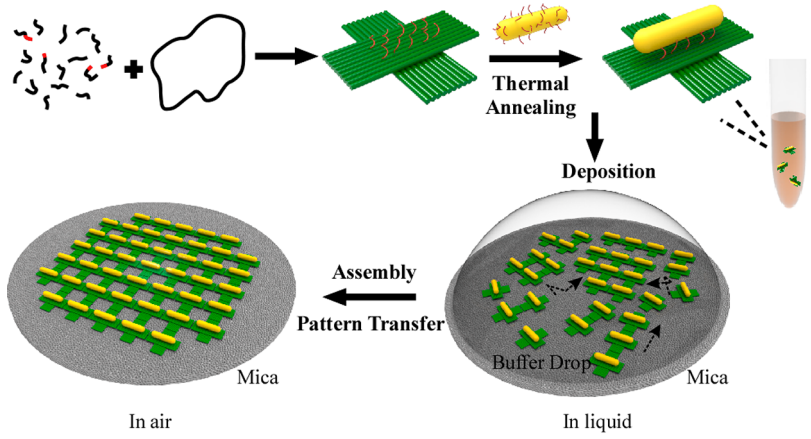

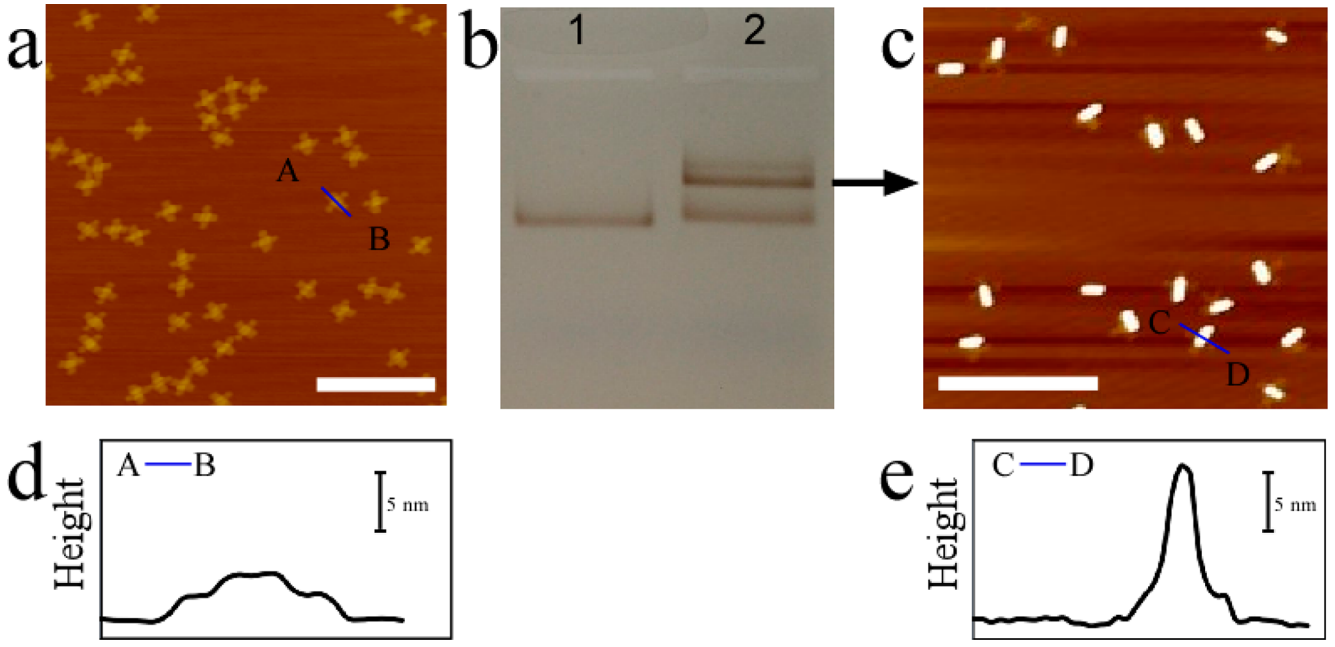

Figure 1. Attachment of AuNRs on DNA origami frame. (a,c) AFM images of DNA origami frames before and after DNA functionalized AuNRs attachment and corresponding section profiles along lines A-B (d) and C−D (e). (b) Agarose gel electrophoresis image of DNA functionalized AuNRs on origami frame. Scale bar, 500 nm.

the interface of liquid and substrates such as mica[26,27] by controlling the concentrations of divalent and monovalent ions, and lipid[28−30] into ordered superstructures. However, to the best of our knowledge, this strategy has not yet been used to assemble DNA origami framed plasmonic nanomaterials on a large scale.

In this study, we combined the surface diffusion-mediated assembly strategy with a pattern transfer method to fabricate well-aligned AuNR clusters and large 1D and 2D arrays. DNA functionalized AuNRs were decorated on DNA origami frames and programmed to assemble into 2D arrays through base-stacking interactions at liquid−solid interfaces. These assembled 2D arrays exhibited excellent stability against aggregation and high yield with AuNRs well arranged in predesigned orientation for the first time. However, the further utilization of these patterns to fabricate nanoelectronic or plasmonic devices was limited as the pattern was formed in wet conditions. Furthermore, we demonstrated that preformed arrays of AuNRs were intactly transferred from liquid environment to dry ambient environment in the pattern transfer process. More complex and larger-scale AuNR arrays were fabricated by assembling on the mica surface with DNA origami as the scaffold. In general, the results represented critical progress toward the large-scale, high-yield, and precise fabrication of metallic nanostructures by DNA origami.

RESULTS

Scheme 1 illustrates the strategy for assembling AuNRs into well-controlled two-dimensional (2D) arrays on a solid surface (mica) by the surface diffusion-mediated DNA origami assembly followed by a pattern transfer step. The cross-shaped DNA origami frame[31] developed by Liu et al. was initially constructed by folding a long circular single-stranded DNA (M13mp18) using hundreds of short-staple stands. The origami frame has four edges, with each edge decorated with blunt-ends for stacking interactions between the origami

https://doi.org/10.1021/acsami.1c13173
ACS Appl. Mater. Interfaces 2021, 13, 50516−50523

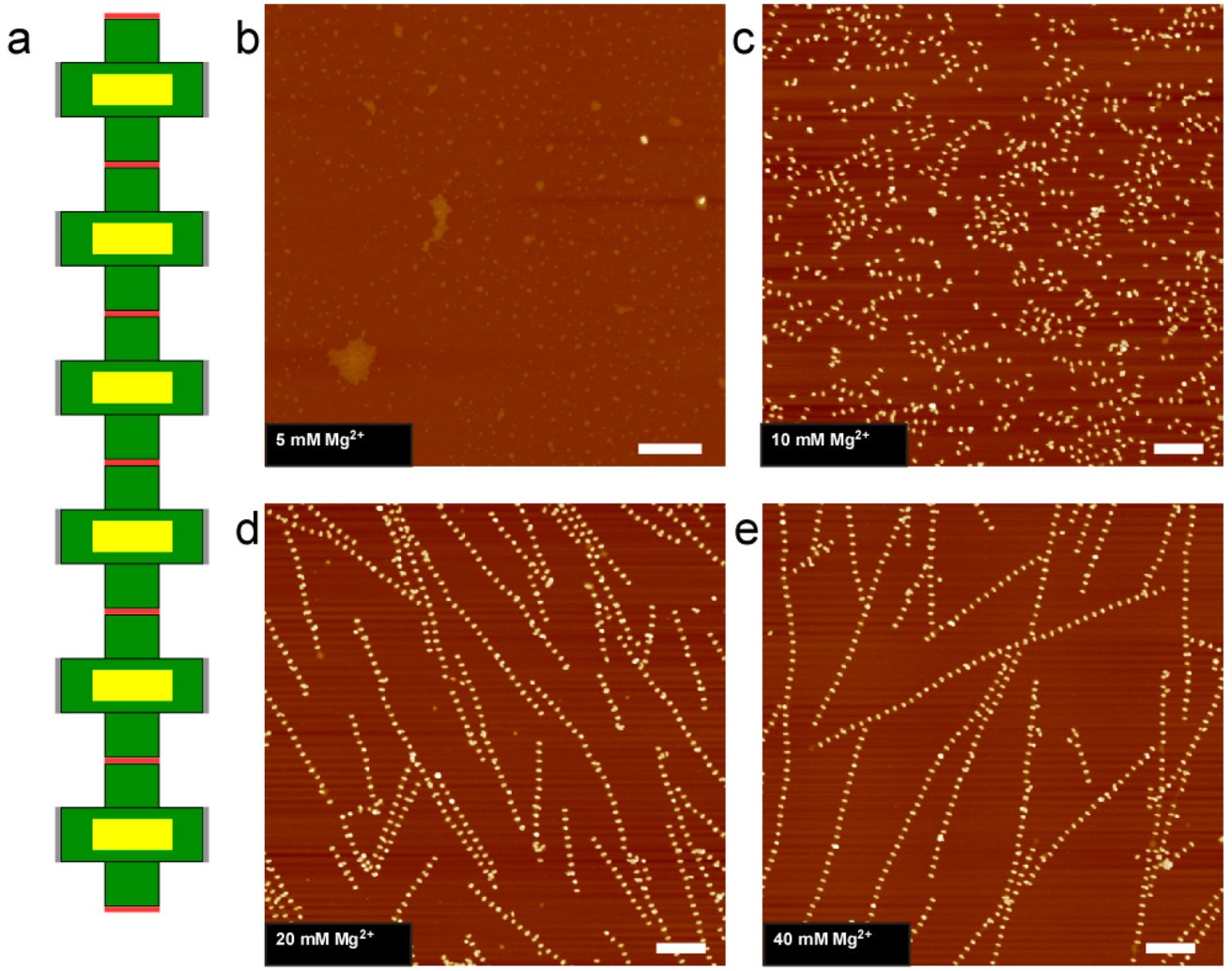

Figure 2. 1D arrays of AuNRs as a function of varying Mg^{2+} concentration during pattern transfer. (a) Schematic drawing of the design of AuNR 1D array in side-by-side configuration. (b–e) AFM images of AuNR 1D arrays with different Mg^{2+} concentration: (b) 5 mM, (c) 10 mM, (d) 20 mM, (e) 40 mM. Scale bar, 500 nm.

frames. To introduce the stacking interactions with uniform strength on the four edges, all the blunt ends were customized with GC base pairs. The structural design is shown in the Supporting Information (SI). The center of each origami frame was designed with one set of 10 single-stranded DNA (ssDNA, red color) as binding sites to anchor AuNRs. Thiolated ssDNA, which had complementary sequences to the ssDNA on origami frame, were decorated on the surface of AuNRs by a salting–aging process.[32−34] The hybridization between binding strands on the origami frame and its complementary ssDNA on AuNRs led to the formation of origami framed AuNRs. The resulting nanostructures were characterized by atomic force microscopy (AFM) and agarose gel electrophoresis (Figure 1). Figure 1a represented the AFM image of the cross-shaped origami, indicating the successful construction of the predesigned structure. Figure 1b shows the gel image, in which lane 1 represented the DNA functionalized AuNRs as control, whereas lane 2 exhibited an intense upper band with slower mobility compared to the extra AuNRs band (bottom band), suggesting the successful attachment of AuNRs on origami frame. In order to further determine the morphology of origami framed AuNRs, the band was extracted and then examined by AFM, as shown in Figure 1c. Comparison between the AFM images of the origami frames (Figure 1a) and the AuNRs on origami frames (Figure 1c) confirmed that AuNRs were successfully decorated on the origami frames, which was consistent with the result from the gel image. However, some AuNRs seemed to be shifted off from the desired binding position, which was very likely coming from the partial hybridization between binding strands on origami frames and ssDNA coated on AuNRs. The section profiles along with the origami frame (A, B in Figure 1a) and AuNRs on the origami frame (C, D in Figure 1c) are shown in Figure 1d, e, respectively. As seen from the results, the height of the profile was increased from 4 to 13 nm, indicating the attachment of AuNRs.

To obtain the origami framed AuNRs into well-ordered 2D arrays in the dry ambient environment, two major steps were conducted. In the first step, called a surface diffusion-mediated assembly, origami framed AuNRs were assembled into arrays on a mica surface in the liquid environment by carefully adjusting the ratio between Mg^{2+} and Na^{+}. Then, in the second step, called the pattern transfer process, the preformed AuNRs arrays were transferred from a wet to dry environment without disturbing the pattern when the balance of cation-controlled interaction was interrupted. In the first step, rather than using

https://doi.org/10.1021/acsami.1c13173
ACS Appl. Mater. Interfaces 2021, 13, 50516−50523

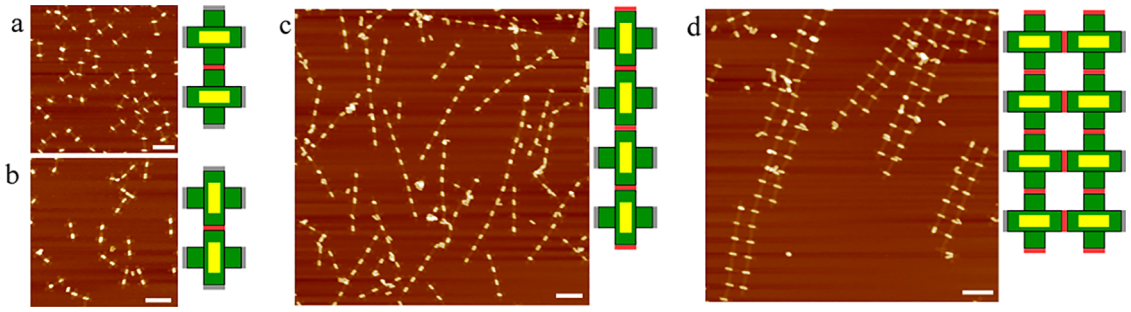

Figure 3. AuNRs dimers and complex AuNRs clusters. (a) AuNRs dimers in end-to-end and (b) side-by-side configurations. (c) 1D arrays of AuNRs in end-to-end configuration. (d) AuNRs ladder arrays. Scale bar, 200 nm.

sticky-strand hybridization between origami frames, we employed blunt-end stacking interactions.[35−37] This type of interaction was weaker and thus allowed reorganization of origami units to grow into larger nanostructures during the surface diffusion-mediated assembly process. The assembly was achieved by controlling the surface mobility of DNA origami frames in the liquid environment through manipulating the concentration of divalent (Mg^{2+}) and monovalent (Na^{+}) cations.[38−41] Under liquid conditions (typically 1× Tris-acetate-EDTA buffer, 10.5 mM Mg^{2+}), DNA origami frames were immobile with strong adhesion to the mica substrate, as was mediated by divalent cation Mg^{2+}. When the monovalent cation Na^{+} was introduced, DNA origami frames became mobile.[38] The origami units with mobility were able to move around on the mica surface and associate into well-ordered arrays. In the assembly process, the concentration of Na^{+} played a critical role in the formation of arrays. In order to investigate the optimized concentration of Na^{+}, origami frames were treated with solutions containing varied concentrations of Na^{+} from 0 mM to 600 mM. As seen from the results in SI Figure S1, [NaCl] = 450 mM was the optimized concentration leading to large DNA origami 2D arrays and was thus chosen for the subsequent studies. After the assembly process, the preformed arrays of origami framed AuNRs with designed patterns in a liquid environment need to be transferred to a dry ambient environment. In this pattern transfer step, any disturbance of the preestablished cation balance will damage the formed structures. Therefore, stronger interactions between mica and origami frames were desired to prevent the AuNRs from structural damage during the removal of the buffer. This was achieved by adding extra Mg^{2+} to stabilize the arrays before rinsing.

To optimize the yield of arrays in the pattern transfer step, we tested how the concentration of Mg^{2+} affected the structure of the 1D arrays of origami framed AuNRs during the pattern transfer (Figure 2). The structural design of the 1D arrays of AuNRs is shown in the schematic drawings of Figure 2a and SI Figure S2. GC pair blunt ends were only designed on the opposite edges (red color) of origami frames while leaving the scaffold loop on the other two sides unpaired (gray color). Such design enabled the stacking interactions to only occur in a linear direction between the origami frames. After sample deposition and following incubation on mica, the 1D arrays of origami framed AuNRs formed in a liquid environment and exhibited blurring shadow in SI Figure S3 because of the unstable nature of AuNR arrays during liquid AFM scanning. In order to increase the binding affinity between AuNR pattern and mica surface while not disturbing the preformed arrays, various concentrations of Mg^{2+} from 5 mM to 40 mM were added to treat the samples for immobilization and pattern transfer processes. As seen from the results, no linear arrays of AuNRs were found after treatment with 1×TAE containing 5 mM Mg^{2+}, suggesting that 5 mM Mg^{2+} was insufficient to immobilize the formed AuNRs array structures on the mica surface during the pattern transfer process (Figure 2b). When the concentration of Mg^{2+} was increased to 10 mM, AuNRs were assembled into the shorter linear array with tile number less than 5 (Figure 2c), indicating 10 mM Mg^{2+} started to improve the immobility of the formed arrays. As the concentration of Mg^{2+} was further increased to 20 mM and 40 mM, much longer AuNRs linear arrays were observed, indicating the concentration of Mg^{2+} was high enough to stabilize the formed arrays with their structures maintained during the pattern transfer process (Figure 2d, e). Since no significant difference in the results by 20 mM Mg^{2+} and 40 mM Mg^{2+} was found, it was determined that Mg^{2+} concentration of 20 mM was sufficient to provide high yield in the pattern transfer process and was thus used for subsequent studies.

With the optimized surface diffusion-mediated assembly and pattern transfer processes, many different types of AuNR arrays were constructed and transferred. First, AuNRs dimers in both end-to-end and side-by-side configurations were designed by placing GC pair blunt ends on the one side (red color) of origami frames while leaving the scaffold loop on the other three sides unpaired (gray color) as shown in the schematic drawings in Figure 3a, b, respectively. Dimer AuNRs were successfully assembled and visualized by AFM. It is worth noting that electrostatic repulsion between DNA-functionalized AuNRs in end-to-end configuration was more potent than that in a side-by-side configuration, which led to the low yield of dimer formation in end-to-end configuration (SI Figure S4). The electrostatic repulsion can be moderated by controlling divalent cations, such as Mg^{2+} in the buffer.[42] Besides that, it is known that the base stacking interactions between origami frames would enhance with higher salt concentration. Thus, the concentration of Mg^{2+} in the assembly process was modified to 15 mM to moderate the electrostatic repulsion and increase stacking interaction. With this modification, the AuNRs dimers in the end-to-end configuration were successfully formed with a high yield, as demonstrated in Figure 3b. Besides AuNRs dimer, complex AuNRs nanoclusters were also constructed, including 1D arrays of AuNRs in both end-to-end and side-by-side configurations and ladder arrays of AuNRs. Interestingly, 1D arrays of AuNRs in side-by-side configuration formed longer 1D arrays with high yield (Figure 2). The average number of AuNRs in 1D arrays is 25 ± 7.0. While the AuNRs in end-to-end configuration assembled into 1D arrays in shorter length

https://doi.org/10.1021/acsami.1c13173
ACS Appl. Mater. Interfaces 2021, 13, 50516−50523

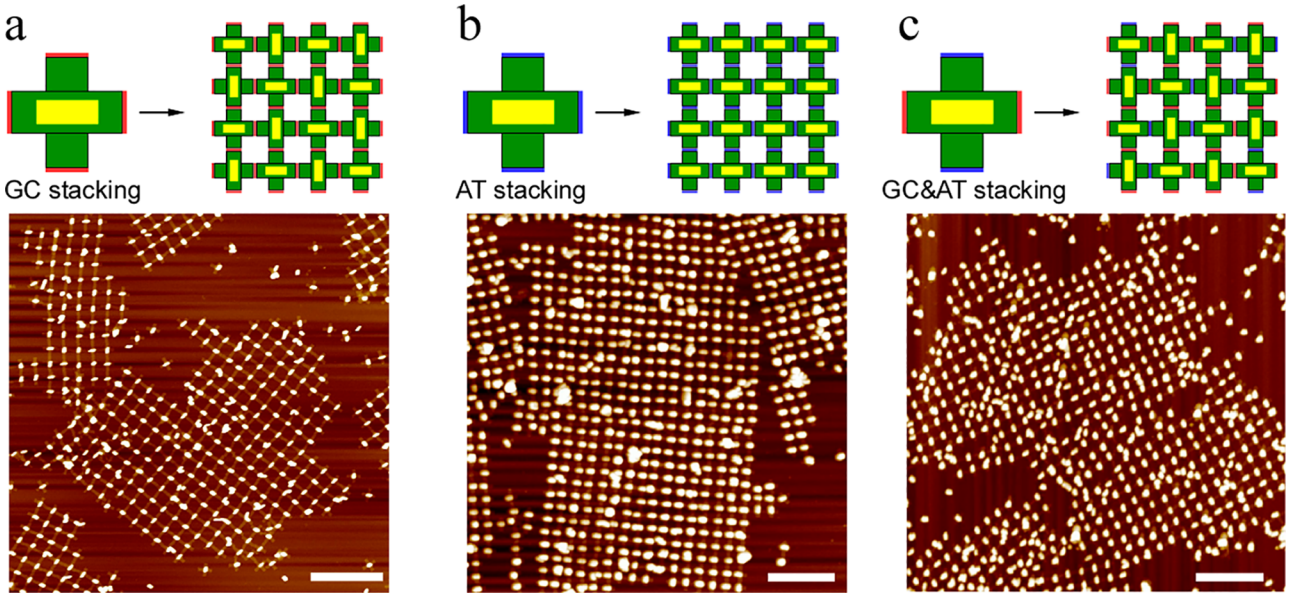

Figure 4. AuNR 2D arrays formed by origami frames with GC stacking (a), AT stacking (b), and both GC stacking and AT stacking (c). Scale bar, 500 nm.

even with modified Mg^{2+} concentration (the average number of AuNRs is 5.2 ± 2.0) (Figure 3c). The length distribution of AuNRs in 1D arrays are shown in SI Figure S5. This may also be attributed to the electrostatic repulsion between DNA-functionalized AuNRs. For AuNRs ladder arrays, three adjacent sides of origami frames were designed with GC pair blunt ends (red color), as shown in the schematic drawing in Figure 3d. Ladder arrays of AuNRs were assembled and visualized as shown in the AFM image in Figure 3d. In addition, the stacking interaction could be introduced on the top and right sides of cross DNA origami, from the AFM image (Figure S6), it can be revealed the origami mainly formed in zigzag shapes. Overall, the results revealed the versatility of the proposed method in the assembly of AuNRs.

Encouraged by the formation of various patterns of AuNRs by the substrate-assisted self-assembly method, we also explored the feasibility of large-scale assembly of 2D arrays of origami-framed AuNRs. It is already known that the strength of stacking interactions would vary according to the binding energy of different sequences in the blunt-ends: with GC pair of −2.17 kcal/mol versus AT pair of −0.19 kcal/mol.[43] Herein, we investigated whether the strength of stacking interactions would affect the orientation of the self-assembly of origami-framed AuNRs by designing different sequences in the blunt-ends. First, the structural design of origami frames for AuNR 2D arrays is shown in the schematic drawings in Figure 4a and SI Figure S7. The four edges of origami frames were fully designed with GC pair blunt ends (red color). Such design enabled the stacking interactions occurring in four directions between the origami frames. As a result, AuNRs were aligned into random patterns due to strong stacking interactions between GC pairs, as seen in the AFM image in Figure 4a. Orientation of the formed AuNR arrays was highlighted, as shown in SI Figure S8. Besides the random pattern assembled via GC stacking, the four edges of origami frames were also modified with weaker blunt-end stacking interactions (AT pair blunt ends).[43] Surprisingly, well-ordered 2D arrays of AuNRs were constructed, shown in Figure 4b. The possible reason is that the GC base pair provides a particularly strong stacking interaction to overcome the electrostatic repulsion of AuNRs and/or the twist defects from DNA origami, which offers the freedom of assembly in four directions leading to the orientation changes of some AuNRs. While the AT base pair has much weaker stacking strength which prefers the formation of the 1D array of AuNRs in side-by-side arrangement first, then extends in other direction, forming the ordered 2D array. In order to figure out the underlying mechanism of the different assembly configurations in Figure 4a, b, we modified the AT pair blunt ends on the left and right sides of origami frames to GC pair blunt ends (Figure 4c). It was found that random patterns rather than well-ordered 2D arrays were formed. The results revealed that by increasing the strength of stacking interactions on the origami frames, stronger electrostatic repulsion between DNA-functionalized AuNRs was moderated, which led to the configuration transformation from well-ordered 2D arrays to the random pattern. The large-scale AFM images of AuNR assembly with GC and AT stacking interactions are shown in SI Figures S9 and S10, respectively. The results demonstrated that programming the strength of stacking between origami structures could control the selective binding between DNA structures.

CONCLUSIONS

In summary, we demonstrated a novel surface diffusion-mediated DNA origami assembly method for the fabrication of plasmonic nanomaterials into well-ordered structures. Highly ordered 1D and 2D arrays of AuNRs were constructed by employing DNA origami frames as scaffolds with the surface mobility of DNA origami in a liquid environment manipulated by divalent (Mg^{2+}) and monovalent (Na^{+}) cations. The assembled 1D and 2D arrays of AuNRs were successfully transferred from liquid environment to dry ambient environment with high yield with optimized Mg^{2+} concentration. The successful assembly of AuNRs dimers, 1D arrays, and ladder arrays of AuNRs in both end-to-end and side-by-side configurations revealed the versatility of the proposed method in the assembly of AuNRs. Well-ordered and micrometer-sized 2D superstructures with AuNRs arranged in a predesigned

https://doi.org/10.1021/acsami.1c13173
ACS Appl. Mater. Interfaces 2021, 13, 50516−50523

orientation demonstrated the scalability of the proposed method. The new origami-assisted surface assembly and pattern transfer strategies could provide a cost-effective and reliable method for organizing AuNRs or other functional materials with promising applications in nanoelectronics and nanoplasmonics and the capability to integrate with many advanced lithography techniques.

EXPERIMENTAL METHODS

Materials. All chemicals were purchased from Sigma and used as received without further purification. All chemically synthesized DNA strands were purchased from Integrated DNA Technologies, Inc. (www.Idtdna.com). The unmodified staple strands were ordered in a 96-well plate format, suspended in ultrapure water without purification.

Preparation of DNA Origami. According to Dr. Rothermund method,[15] M13mp18 viral DNA and all of the staple strands were mixed at a ratio of 1:5 in 1 × TAE buffer solution containing 40 mM Tris-HCl, 20 mM acetic acid, 2 mM of EDTA, and 11.5 mM magnesium acetate. The mixture was slowly cooled from 90 °C to 15 °C with a thermal cycler over 12h. The final concentration of M13mp18 DNA in the solution was 20 nM.

Synthesis of gold nanorods. Gold nanorods were prepared according to the seed-mediated growth method described by EI-Sayed et al.[44]

1. AuNRs Seed Solution. Five mL of 0.5 mM $HAuCl_4$ solution was mixed with 5 mL of 0.2 M of CTAB solution. Under vigorous stirring, 0.6 mL of 10 mM freshly prepared, ice-cold $NaBH_4$ was added into the mixture. The color of the solution quickly changed to brown-yellow, and the mixture was kept under vigorous stirring for 2 min. The resulting AuNR seed solution acted as nucleation sites for AuNRs growth.

2. AuNRs Growth. In a 250 mL Erlenmeyer flash, 1.2 mL of $AgNO_3$ solution (10 mM) was added into 200 mL of CTAB solution (0.1 M) with stirring. After 10 min, 5 mL of $HAuCl_4 \cdot 3H_2O$ solution (10 mM) was added into the flask. After another 3 min, 0.6 mL of L-ascorbic acid solution (0.1M) was added to the above mixture with gentle stirring until the solution color changed to colorless. Then 400 μL of seed solution was added into the flask under vigorous stirring for the 30s and left undisturbed at 27 °C overnight for AuNRs growth. The AuNR solution was centrifuged for 30 min before using to remove extra CTAB.

Preparation of DNA Functionalized Gold Nanorods. Gold nanorods were functionalized with thiolated DNA. Prior to use, the SH-DNA was cleaved by adding TCEP and incubated at room temperature for 1 h. The cleaved oligonucleotides were purified using a G-25 column. Freshly cleaved oligonucleotides were added to gold nanorod solutions with molar ratios of 500:1. 0.01% sodium dodecyl sulfate (SDS) was added to gold nanorods solutions. The oligonucleotide/gold nanorods solution was allowed to incubate at room temperature for 1 h. The concentration of NaCl was increased to 50 mM, using 2 M NaCl, 0.01 M PBS, during a 12 h period. The gold nanoparticles were centrifuged to remove excess DNA, and the supernatant was removed, leaving a pellet of gold nanoparticles at the bottom. The particles were then suspended in a PBS buffer containing 25 mM of NaCl. This washing process was repeated three times, and then the gold nanoparticles were dispersed in a PBS buffer and measured by UV−vis.

Formation of DNA Origami Framed AuNRs. The prepared origami frames were mixed with AuNRs at a molar ratio of 1:3 in a 1×TAE buffer containing 11.5 mM of magnesium acetate, followed by annealing from 50 °C to 30 °C over 12h time course.

Formation of 2D arrays of DNA Origami Frames. Five μL of origami solution (20 nM) was diluted with 100 μL 1×TAE buffer containing 11.5 mM of magnesium acetate and 450 mM of sodium chloride, and then deposited on freshly cleaved mica. The sample was incubated for 12 h at room temperature in a sealed container. After incubation, the morphology of the sample was visualized by AFM.

Pattern Transfer Method. 100 μL of origami solution (1 nM) in 1xTAE buffer containing 11.5 mM of magnesium acetate and 450 mM of NaCl was deposited on freshly cleaved mica for 12 h for substrate-assisted self-assembly and incubated in a sealed container to keep humid. After incubation, the remaining buffer on the mica was gently wicked off by a piece of Kimwipe. 150 μL of 1xTAE with 20 mM of magnesium acetate was deposited on mica to immobilize the preformed structures. After immobilization for 30s, the solution was wicked off. Next, double- distilled H_2O (50 μL) was dropped on the mica to remove the buffer salts, then the drop was wicked off. The rinsing step was repeated three times. Lastly, the sample was dried with compressed air.

AFM Imaging. The AFM images were obtained using the Bruker Dimension Icon instrument.

For samples in drying conditions, spotting the sample (3 μL) onto freshly cleaved muscovite mica (Ted Pella, Inc.) for 15 s. After the fixation of the targeted structure of DNA origami on the mica surface, double-distilled H_2O (50 μL) was dropped on the mica to remove the buffer salts, then the drop was wicked off, and the sample was dried with compressed air. Atomic force imaging was done by utilizing ScanAsyst mode in air, with ultrasharp 14 series (NSC 14) tips purchased from NANOANDMORE.

For samples in liquid conditions, 5 μL of sample solution was mixed with 100 μL 1xTAE buffer containing 450 mM NaCl and deposited on freshly cleaved mica for mica-assisted self-assembly. Atomic force imaging was done by utilizing ScanAsyst-fluid mode with ScanAsyst-fluid probes from Bruker.

Agarose Gel Electrophoresis. For the agarose gel, the samples were loaded into 0.8% agarose gel that contained 5 mM $Mg(CH_3COO)_2$ in a 1 × TAE buffer solution under 55 V at room temperature. The gel was stained with ethidium bromide for visualization.

ASSOCIATED CONTENT

Supporting Information

The Supporting Information is available free of charge at https://pubs.acs.org/doi/10.1021/acsami.1c13173.

AFM images, structural design, and DNA sequences (PDF)

AUTHOR INFORMATION

Corresponding Author

Risheng Wang − *Department of Chemistry, Missouri University of Science and Technology, Rolla, Missouri 65409, United States;* orcid.org/0000-0001-6539-1565; Email: wangri@mst.edu

Authors

Shuo Yang − *Department of Chemistry, Missouri University of Science and Technology, Rolla, Missouri 65409, United States*

Wenyan Liu − *Department of Chemistry and Center for Research in Energy and Environment, Missouri University of Science and Technology, Rolla, Missouri 65409, United States*

Yuwei Zhang − *Department of Chemistry, Missouri University of Science and Technology, Rolla, Missouri 65409, United States*

Complete contact information is available at: https://pubs.acs.org/10.1021/acsami.1c13173

Notes

The authors declare no competing financial interest.

■ ACKNOWLEDGMENTS

This work was supported by the National Science Foundation under grants CCF-1814797, and Office of Research, Missouri University of Science and Technology.

■ REFERENCES

(1) Simon, U. Nanoparticle self-assembly: Bonding them all. *Nat. Mater.* **2013**, *12*, 694−696.
(2) Li, N.; Zhao, P.; Astruc, D. Anisotropic gold nanoparticles: Synthesis, properties, applications, and toxicity. *Angew. Chem., Int. Ed.* **2014**, *53*, 1756−1789.
(3) Ma, W.; Kuang, H.; Xu, L.; Ding, L.; Xu, C.; Wang, L.; Kotov, N. A. Attomolar DNA detection with chiral nanorod assemblies. *Nat. Commun.* **2013**, *4*, 2689.
(4) Nie, Z.; Fava, D.; Kumacheva, E.; Zou, S.; Walker, G. C.; Rubinstein, M. Self-assembly of metal-polymer analogues of amphiphilic triblock copolymers. *Nat. Mater.* **2007**, *6*, 609−614.
(5) Vittala, S. K.; Han, D. DNA-Guided Assemblies toward Nanoelectronic Applications. *ACS Appl. Bio Mater.* **2020**, *3*, 2702−2722.
(6) Seeman, N. C.; Sleiman, H. F. DNA nanotechnology. *Nat. Rev. Mater.* **2018**, *3*, 17068.
(7) Raveendran, M.; Lee, A. J.; Sharma, R.; Wälti, C.; Actis, P. Rational design of DNA nanostructures for single molecule biosensing. *Nat. Commun.* **2020**, *11*, 1−9.
(8) Han, S.; Liu, W.; Yang, S.; Wang, R. Facile and Label-Free Electrochemical Biosensors for MicroRNA Detection Based on DNA Origami Nanostructures. *ACS Omega* **2019**, *4*, 11025−11031.
(9) Schüller, V. J.; Heidegger, S.; Sandholzer, N.; Nickels, P. C.; Suhartha, N. A.; Endres, S.; Bourquin, C.; Liedl, T. Cellular immunostimulation by CpG-sequence-coated DNA origami structures. *ACS Nano* **2011**, *5*, 9696−9702.
(10) Douglas, S. M.; Bachelet, I.; Church, G. M. A Logic-Gated Nanorobot for Targeted Transport of Molecular Payloads. *Science* **2012**, *335*, 831−834.
(11) Zeng, Y.; Liu, J.; Yang, S.; Liu, W.; Xu, L.; Wang, R. Time-lapse live cell imaging to monitor doxorubicin release from DNA origami nanostructures. *J. Mater. Chem. B* **2018**, *6*, 1605−1612.
(12) Liu, J.; Geng, Y.; Pound, E.; Gyawali, S.; Ashton, J. R.; Hickey, J.; Woolley, A. T.; Harb, J. N. Metallization of branched DNA origami for nanoelectronic circuit fabrication. *ACS Nano* **2011**, *5*, 2240−2247.
(13) Ye, J.; Helmi, S.; Teske, J.; Seidel, R. Fabrication of Metal Nanostructures with Programmable Length and Patterns Using a Modular DNA Platform. *Nano Lett.* **2019**, *19*, 2707−2714.
(14) Bayrak, T.; Helmi, S.; Ye, J.; Kauert, D.; Kelling, J.; Schönherr, T.; Weichelt, R.; Erbe, A.; Seidel, R. DNA-Mold Templated Assembly of Conductive Gold Nanowires. *Nano Lett.* **2018**, *18*, 2116−2123.
(15) Rothemund, P. W. K. Folding DNA to create nanoscale shapes and patterns. *Nature* **2006**, *440*, 297−302.
(16) Kuzyk, A.; Jungmann, R.; Acuna, G. P.; Liu, N. DNA Origami Route for Nanophotonics. *ACS Photonics* **2018**, *5*, 115−1163.
(17) Liu, N.; Liedl, T. DNA-Assembled Advanced Plasmonic Architectures. *Chem. Rev.* **2018**, *118*, 3032−3053.
(18) Wang, P.; Huh, J. H.; Park, H.; Yang, D.; Zhang, Y.; Zhang, Y.; Lee, J.; Lee, S.; Ke, Y. DNA Origami Guided Self-Assembly of Plasmonic Polymers with Robust Long-Range Plasmonic Resonance. *Nano Lett.* **2020**, *20*, 8926−8932.
(19) Lan, X.; Liu, T.; Wang, Z.; Govorov, A. O.; Yan, H.; Liu, Y. DNA-Guided Plasmonic Helix with Switchable Chirality. *J. Am. Chem. Soc.* **2018**, *140*, 11763−11770.
(20) Zhou, C.; Duan, X.; Liu, N. A plasmonic nanorod that walks on DNA origami. *Nat. Commun.* **2015**, *6*, 8102.
(21) Zhan, P.; Dutta, P. K.; Wang, P.; Song, G.; Dai, M.; Zhao, S. X.; Wang, Z. G.; Yin, P.; Zhang, W.; Ding, B.; Ke, Y. Reconfigurable Three-Dimensional Gold Nanorod Plasmonic Nanostructures Organized on DNA Origami Tripod. *ACS Nano* **2017**, *11*, 1172−1179.
(22) Liu, W.; Li, L.; Yang, S.; Gao, J.; Wang, R. Self-Assembly of Heterogeneously Shaped Nanoparticles into Plasmonic Metamolecules on DNA Origami. *Chem. - Eur. J.* **2017**, *23*, 14177−14181.
(23) Yang, S.; Liu, W.; Wang, R. Control of the stepwise assembly-disassembly of DNA origami nanoclusters by pH stimuli-responsive DNA triplexes. *Nanoscale* **2019**, *11*, 18026−18030.
(24) Sun, X.; Hyeon Ko, S.; Zhang, C.; Ribbe, A. E.; Mao, C. Surface-Mediated DNA Self-Assembly. *J. Am. Chem. Soc.* **2009**, *131*, 13248−13249.
(25) Hamada, S.; Murata, S. Substrate-Assisted Assembly of Interconnected Single-Duplex DNA Nanostructures. *Angew. Chem.* **2009**, *121*, 6952−6955.
(26) Aghebat Rafat, A.; Pirzer, T.; Scheible, M. B.; Kostina, A.; Simmel, F. C. Surface-assisted large-scale ordering of DNA origami tiles. *Angew. Chem., Int. Ed.* **2014**, *53*, 7665−7668.
(27) Woo, S.; Rothemund, P. W. K. Self-assembly of two-dimensional DNA origami lattices using cation-controlled surface diffusion. *Nat. Commun.* **2014**, *5*, 4889.
(28) Suzuki, Y.; Endo, M.; Sugiyama, H. Lipid-bilayer-assisted two-dimensional self-assembly of DNA origami nanostructures. *Nat. Commun.* **2015**, *6*, 1−9.
(29) Kocabey, S.; Kempter, S.; List, J.; Xing, Y.; Bae, W.; Schiffels, D.; Shih, W. M.; Simmel, F. C.; Liedl, T. Membrane-Assisted Growth of DNA Origami Nanostructure Arrays. *ACS Nano* **2015**, *9*, 3530−3539.
(30) Kempter, S.; Khmelinskaia, A.; Strauss, M. T.; Schwille, P.; Jungmann, R.; Liedl, T.; Bae, W. Single particle tracking and super-resolution imaging of membrane-assisted stop-and-go diffusion and lattice assembly of DNA origami. *ACS Nano* **2019**, *13*, 996−1002.
(31) Liu, W.; Zhong, H.; Wang, R.; Seeman, N. C. Crystalline two-dimensional DNA-origami arrays. *Angew. Chem., Int. Ed.* **2011**, *50*, 264−267.
(32) Liu, J.; Lu, Y. Preparation of aptamer-linked gold nanoparticle purple aggregates for colorimetric sensing of analytes. *Nat. Protoc.* **2006**, *1*, 246−252.
(33) Hill, H. D.; Mirkin, C. A. The bio-barcode assay for the detection of protein and nucleic acid targets using DTT-induced ligand exchange. *Nat. Protoc.* **2006**, *1*, 324−336.
(34) Huang, Y.; Nguyen, M. K.; Kuzyk, A. Assembly of Gold Nanorods into Chiral Plasmonic Metamolecules Using DNA Origami Templates. *J. Visualized Exp.* **2019**, *145*, 1−8.
(35) Gerling, T.; Wagenbauer, K. F.; Neuner, A. M.; Dietz, H. Dynamic DNA Devices and Assemblies Formed by Shape-Complementary, non-Base Paring 3D Components. *Science* **2015**, *347*, 1446−1452.
(36) Kilchherr, F.; Wachauf, C.; Pelz, B.; Rief, M.; Zacharias, M.; Dietz, H. Single-Molecule Dissection of Stacking Forces in DNA. *Science* **2016**, *353*, 6304.
(37) Woo, S.; Rothemund, P. W. K. Programmable Molecular Recognition Based on the Geometry of DNA Nanostructures. *Nat. Chem.* **2011**, *3*, 620−627.
(38) Pastré, D.; Piétrement, O.; Fusil, S.; Landousy, F.; Jeusset, J.; David, M. O.; Hamon, L.; Le Cam, E.; Zozime, A. Adsorption of DNA to mica mediated by divalent counterions: A theoretical and experimental study. *Biophys. J.* **2003**, *85*, 2507−2518.
(39) Pastré, D.; Hamon, L.; Landousy, F.; Sorel, I.; David, M. O.; Zozime, A.; Le Cam, E.; Piétrement, O. Anionic polyelectrolyte adsorption on mica mediated by multivalent cations: A solution to DNA imaging by atomic force microscopy under high ionic strengths. *Langmuir* **2006**, *22*, 6651−6660.
(40) Bezanilla, M.; Manne, S.; Laney, D. E.; Lyubchenko, Y. L.; Hansma, H. G. Adsorption of DNA to Mica, Silylated Mica, and Minerals: Characterization by Atomic Force Microscopy. *Langmuir* **1995**, *11*, 655−659.
(41) Xin, Y.; Rivadeneira, S. M.; Grundmeier, G.; Castro, M.; Keller, A. Self-assembly of highly ordered DNA origami lattices at solid-liquid interfaces by controlling cation binding and exchange. *Nano Res.* **2020**, *13*, 3142−3150.

(42) Misra, V. K.; Draper, D. E. The interpretation of Mg^{2+} binding isotherms for nucleic acids using Poisson-Boltzmann theory. *J. Mol. Biol.* **1999**, *294*, 1135−1147.
(43) Protozanova, E.; Yakovchuk, P.; Frank-Kamenetskii, M. D. Stacked-unstacked equilibrium at the nick site of DNA. *J. Mol. Biol.* **2004**, *342*, 775−785.
(44) Nikoobakht, B.; El-Sayed, M. A. Preparation and Growth Mechanism of Gold Nanorods using Seed-Mediated Growth Method. *Chem. Mater.* **2003**, *15*, 1957−1962.

https://doi.org/10.1021/acsami.1c13173
ACS Appl. Mater. Interfaces 2021, 13, 50516−50523